

# Extremely Correlated Fermi Liquid Description of Normal State ARPES in Cuprates

G.-H. Gweon,<sup>1,\*</sup> B. S. Shastry,<sup>1,†</sup> and G. D. Gu<sup>2</sup>

<sup>1</sup>*Physics Department, University of California, Santa Cruz, CA, 95064, USA*

<sup>2</sup>*Condensed Matter Physics and Materials Science Department,  
Brookhaven National Laboratory, Upton, New York 11973, USA*

(Dated: November 29, 2018)

The normal state single particle spectral function of the high temperature superconducting cuprates, measured by the angle resolved photoelectron spectroscopy (ARPES), has been considered both anomalous and crucial to understand. Here we show that an unprecedentedly detailed description of the data is provided by a spectral function arising from the Extremely Correlated Fermi Liquid state of the  $t$ - $J$  model proposed recently by Shastry. The description encompasses both laser and conventional synchrotron ARPES data on optimally doped  $\text{Bi}_2\text{Sr}_2\text{CaCu}_2\text{O}_{8+\delta}$ , and also conventional synchrotron ARPES data on the  $\text{La}_{1.85}\text{Sr}_{0.15}\text{CuO}_4$  materials. *It fits all data sets with the same physical parameter values*, satisfies the particle sum rule and successfully addresses two widely discussed “kink” anomalies in the dispersion.

PACS numbers: 71.10.Ay, 74.25.Jb, 74.72.Gh, 79.60.-i

Angle resolved photo-electron spectroscopy (ARPES) was the first probe to provide a detailed view of the anomalous nature of high temperature cuprate superconductors, discovering unexpectedly broad spectra with intense and asymmetric tails that have remained an enduring mystery for the last two decades. Conventional data taken with high energy ( $\gtrsim 15$  eV) photons from synchrotron light sources have recently been supplemented with laser ARPES data [1, 2] from lower energy (6 or 7 eV) sources. The latter show considerably sharper features near the Fermi energy. A drastic possibility to account for this distinction is that the sudden approximation could break down for the smaller photon energies used in laser ARPES [3]

An important un-answered question is whether the results of the two spectroscopies could be reconciled in a single theoretical framework that does not abandon the sudden approximation. More broadly, can we understand the wide variety of observed lines shapes in a theoretical framework with a sound microscopic basis and a *single* set of parameters?

In this Letter, we confront a recent theory of Extremely Correlated Fermi Liquids (ECFL) proposed by Shastry [4] with the above challenge. The new formalism is complex and requires considerable further effort to yield numerical results in low dimensions. In the limit of high enough dimensions, however, a remarkably simple expression for the Green’s function emerges; it is significantly different from the standard Fermi Liquid Dyson form, while satisfying the usual sum rules. We use the above simple version of ECFL Green’s function in this Letter, motivated by the attractive spectral shapes that it produces with very few parameters [4]. *In this Letter we show that already the simplest version of the ECFL theory, with very few parameters, is successful to an unprecedented extent in detailed fitting of a wide variety of normal state cuprate ARPES line shapes.* Interesting

predictions are made for the higher temperature spectral line skew.

Our focus in this Letter is on the data of optimally doped  $\text{Bi}_2\text{Sr}_2\text{CaCu}_2\text{O}_{8+\delta}$  (Bi2212) and  $\text{La}_{1.85}\text{Sr}_{0.15}\text{CuO}_4$  (LSCO) superconductors in the normal state, taken with  $\vec{k}$  along the nodal direction connecting  $(0,0)$  to  $(\pi/a, \pi/a)$ . Most of the data is taken from the published literature, while some original data are also presented (Bi2212 data in Figs. 4,5). Our sample is an optimally doped Bi2212 ( $T_c = 91$  K), grown by the floating zone method at the Brookhaven National Laboratory (BNL), and was measured at the Stanford Synchrotron Radiation Laboratory (SSRL) beam line 5-4 using 25 eV photons. The energy resolution is 15 meV and the angular resolution is 0.3 degrees.

**Line shape model:** The ECFL spectral function is given as a product of an auxiliary Fermi Liquid (aux-FL) spectral function  $A_{FL}(\vec{k}, \omega)$  and a second frequency dependent “caparison” factor [4, 5]:

$$A(\vec{k}, \omega) = A_{FL}(\vec{k}, \omega) \left( 1 - \frac{n}{2} + \frac{n^2}{4} \cdot \frac{\xi_{\vec{k}} - \omega}{\Delta_0} \right)_+ \quad (1)$$

where  $n$  is the number of electrons per  $\text{CuO}_2$  unit cell,  $(X)_+ \equiv \max(X, 0)$ ,  $\xi_{\vec{k}} = (1 - \frac{n}{2}) \varepsilon(\vec{k})$ , where  $\varepsilon(\vec{k})$  is the bare one-electron band dispersion (see later).  $A_{FL}$  is taken as

$$A_{FL}(\vec{k}, \omega) = \frac{1}{\pi} \cdot \frac{1}{\omega - \xi_{\vec{k}} - \Phi(\omega)} \quad (2)$$

$$\Im \Phi(\omega) = \frac{\omega^2 + \tau^2}{\Omega_0} \exp\left(-\frac{\omega^2 + \tau^2}{\omega_0^2}\right) + \eta, \quad (3)$$

where  $\tau = \pi k_B T$ ,  $T$  is the temperature. From  $\Re \Phi$  [6], the quasi-particle weight of the aux-FL is given by

$$Z_{FL} = \left( 1 + \frac{\omega_0}{\sqrt{\pi} \Omega_0} \right)^{-1} \quad (4)$$

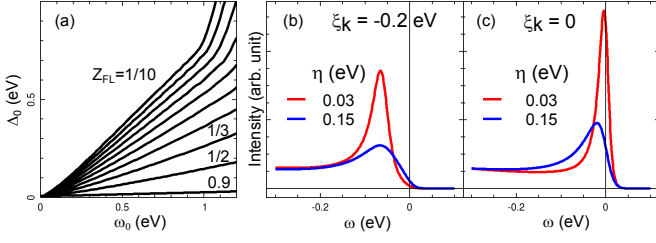


FIG. 1. (a)  $\Delta_0$  as a function of  $\omega_0$  for various  $Z_{FL}$ . Other primary ECFL parameter values are  $n = 0.85$ ,  $T = 100$  K, and  $\xi_{\vec{k}}$  as described in the text. A small  $\eta$  value, 0.010 eV, was used for this plot, which is used as a “lookup table” during the fit. (b,c) Examples of the spectral function calculated with different values of the *effective sample quality parameter*  $\eta$ . See the caption of the next figure for parameter values used. The instrumental energy broadening of 10 meV (FWHM) is included.

The important energy scale  $\Delta_0$  measures the “average intrinsic in-elasticity” of the aux-FL. It is given [4] as:

$$\Delta_0 = \int_{-\infty}^{\infty} d\omega f(\omega) \langle A_{FL}(\vec{k}, \omega) (\xi_{\vec{k}} - \omega) \rangle_{BZ} \quad (5)$$

where  $\langle \cdot \rangle_{BZ}$  denotes averaging over the first Brillouin zone.

The parameters that enter this description are now listed. The “primary parameters” defining the ECFL fit consist of the dispersion  $\xi_{\vec{k}}$  taken from band theory, the density  $n$ , temperature  $T$ , and the aux-FL parameters  $\Delta_0$ ,  $\omega_0$ ,  $Z_{FL}$ ,  $\Omega_0$ . Of the last four parameters, only two are free parameters. For instance,  $\omega_0$  and  $Z_{FL}$  can be taken as free parameters, and  $\Omega_0$  and  $\Delta_0$  can be calculated using Eqs. 4 and 5, respectively.

The parameter  $\eta$  in Eq. (3) is an additional “secondary parameter” [7] with respect to the ECFL theory [4]. Its origin is in impurity scattering as argued in [8], and additionally, in scattering with surface imperfections. Our fits determine  $\eta \approx 0.03$  eV for laser ARPES and  $\eta \approx 0.15$  eV for conventional ARPES. Greater sample penetration of photons in laser ARPES suggests that it should be *less sensitive to surface imperfections* as compared to conventional ARPES, thereby yielding a smaller  $\eta$ . We therefore propose that this parameter summarizes the *effective sample quality* in different experiments. The difference in line shapes arising from these values of  $\eta$  is demonstrated in Figs. 1(b,c).

Our strategy is to fix a common set of intrinsic parameters for all the materials, and allow  $\eta$  to be determined separately for each class of data. The most time consuming part is the calculation of  $\Delta_0$ , the results of which are summarized in Fig. 1(a).

In our line shape analysis (1) we first set  $n = 0.85$ , corresponding to the optimal doping. (2) Here  $\xi_{\vec{k}}$  is taken to be the un-renormalized band dispersion, taken from the literature [9], and then scaled to fit the observed occupied band width, 1.5 eV, of the Bi2212 ARPES result

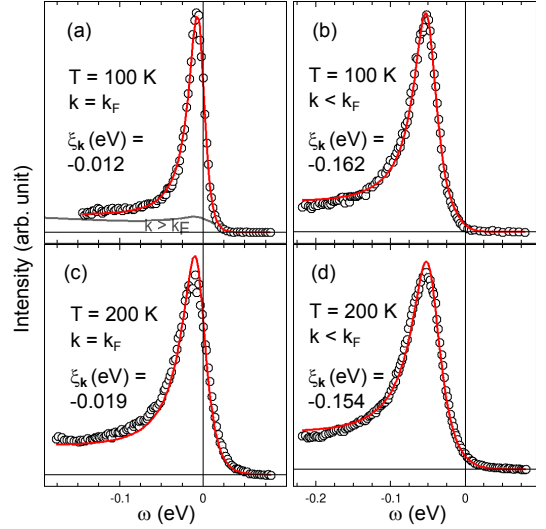


FIG. 2. Laser ARPES data (symbols) from Ref. 14 fit with the ECFL line shape (red lines). The free parameters of the fit were  $\omega_0$  (0.5 eV),  $\eta$  (0.032 eV), and  $\xi_{\vec{k}}$  (shown). Fixed parameters were  $n$  (0.85),  $Z_{FL}$  (1/3). Derived parameters were  $\Delta_0$  (0.12 eV),  $\Omega_0$  (0.14 eV). Other than  $\eta$  and  $\xi_{\vec{k}}$ , the same parameters are used elsewhere in the Letter. In (a), the gray line corresponds to the theoretical curve with  $\xi_{\vec{k}} = 0.15$  eV.

[10][11]. (3) We choose  $Z_{FL} = 1/3$ , to account for the dispersion renormalization due to the high energy kink [10, 12], which in this theory is caused by the energy scale  $\omega_0$  (cf. Fig. 5). (4) Finally, in all simulations, we include the finite energy resolution effect and the finite angle resolution effect as a combined Gaussian broadening (10 meV FWHM for laser ARPES and 25 meV FWHM for conventional ARPES) in energy [13].

**Line shape fit for laser ARPES:** Fig. 2 shows the fit of the laser ARPES data with the ECFL line shape. These fits were made using a procedure that is somewhat more restrictive than that in the recent work of Casey and Anderson invoking the X-ray edge singularity ideas of Doniach and Sunjic (CADS) [14]: we are using global, rather than per-spectrum, fit parameters. However, our fit is somewhat less restricted than other fits shown in this Letter: here we allow a small variation of  $\xi_{\vec{k}}$  as in Ref. 14. We find an excellent fit quality, at least comparable to CADS [14], without having to subtract any extrinsic background intensity. The gray line in panel (a) shows our calculation for  $k > k_F$ . Our expectation is that, were the data for  $k > k_F$  available, we would find a reasonable fit in this  $k$  region as well [15], as for other data sets below.

**Line shape fit for conventional ARPES:** Turning to the conventional ARPES data, we find that the magnitude of the parameter  $\omega_0$  (0.5 eV) determined from the fit of the sharp laser data works very well also for the conventional ARPES data [17]. Thus, for the fit of the

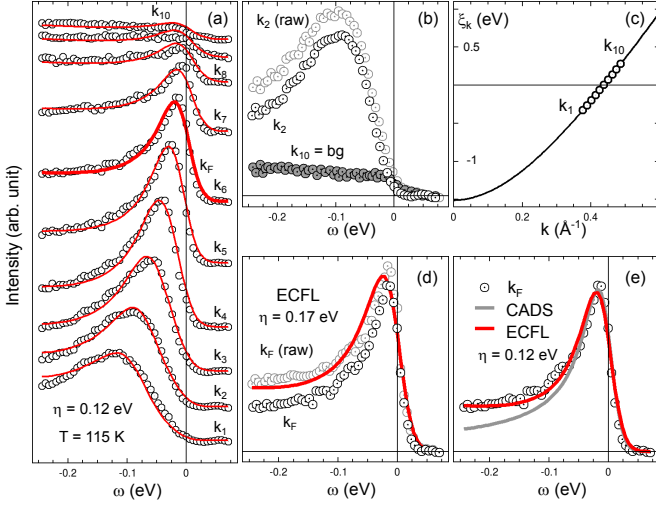


FIG. 3. Conventional ARPES data fit with the ECFL line shape. The data are from Ref. 16 ( $T_c = 90$  K). (a) The data (symbols) and the fit (red lines) are shifted vertically by the same amount for ease of view. (b) An example of the raw data and the fit data is shown for  $k_2$ . The bg (background) spectrum representing the extrinsic background intensity was determined as the raw data at  $k_{10}$ , scaled by 1/2 (“bg scaling factor”). This bg spectrum was subtracted from each raw data, and the resulting data, shown in panel (a), are then fit. (c) The fixed  $\xi_k$  parameters used for the fit. Thus, in this figure,  $\eta$  is the only fit parameter (cf. Fig. 2 caption). (d) Raw data at  $k = k_F$  fit with a somewhat greater  $\eta$  value. (e) The current fit compared with a fit using the CADS line shape.

conventional ARPES data, all parameters other than  $\eta$  are the same. We allow one small exception in Fig. 4(d), where a slight change in  $\omega_0$  produces a much better fit over a larger energy range for LSCO.

Fig. 3 shows our fit of the data in Ref. 16 with a single free parameter  $\eta$ . The amount of the “extrinsic background” (bg) in ARPES is an issue of importance [18–20], especially when analyzing the conventional ARPES data. Here we fit the background subtracted data, as well as the raw data (panel d). For subtracting the background, we use an often-used procedure [20, 21] of equating the background to a fraction (“bg scaling factor”) of the data far beyond the Fermi surface crossing ( $k = k_{10}$  for this data set). The bg scaling factor is determined to be the maximum value for which the resulting intensity is not negative. As shown in the panel d, the ECFL fit remains good by adjusting  $\eta$ , whether or not the extrinsic background is subtracted. In contrast, we find that the CADS theory cannot cope with even the background subtracted data (panel e), giving too steep a fall off towards the left. Likewise, the MFL fits [8, 22] have been shown to compare well with the data only after substantial background subtraction [21, 23].

Our own data on Bi2212 data, taken at  $T_c$  and well

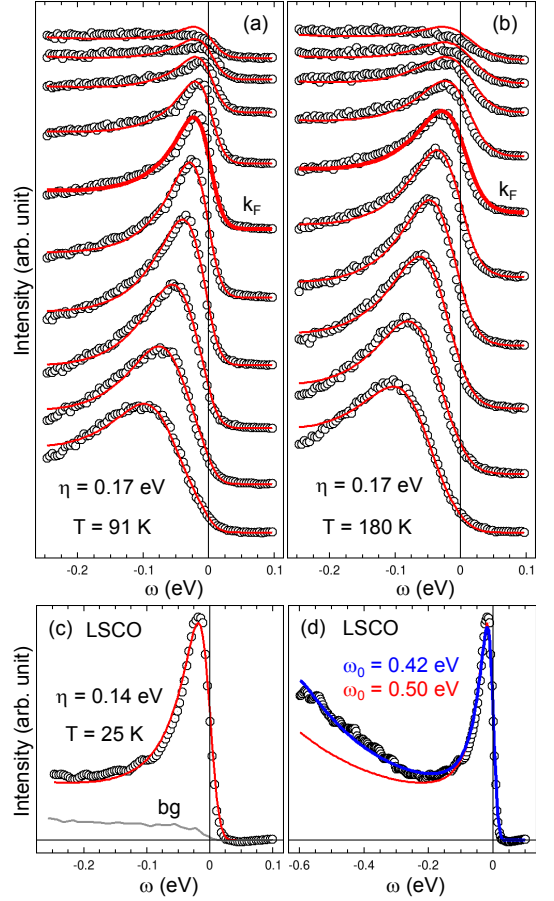


FIG. 4. Conventional ARPES data fit with the ECFL line shape. The procedure used to fit these data are identical with those of the previous figure, i.e. a fit with a single free parameter  $\eta$ , with (d) being a single exception. (a, b) Optimally doped Bi2212 ( $T_c = 91$  K). (c) Optimally doped LSCO data [24, 25]. (d) A test fit up to 0.6 eV for the LSCO data with a small change to  $\omega_0$  for the same data as in (c) but over a wider energy range. On change of the single fit parameter  $\omega_0$  from 0.50 eV to 0.42 eV, an excellent fit up to 0.6 eV can be found. The LSCO data, as far as we are aware, is fit only by the ECFL theory, since an energy dependence rising linearly for occupied states occurs naturally and uniquely in the ECFL spectral function.

above  $T_c$ , can be fit equally well with the same background subtraction procedure, i.e. with the “bg scaling factor” (1/2). The data and the fit are shown in Fig. 4.

We also find that the data for a lower- $T_c$  cuprate LSCO can be fit very well with the same intrinsic parameters. Here, we shall discuss only the  $k = k_F$  data for brevity. In this case, we determine that the “bg scaling factor” be 1 [26]. The subtracted “bg” data [24, 25] is shown as the gray curve in Fig. 4(c). Given their weak superconductivity features [24, 25], these LSCO data are taken to represent the normal state property even if the temperature is slightly lower than  $T_c$ . As for the Bi2212 case, the data can be fit well even without the background subtraction.

tion, if a somewhat greater  $\eta$  value ( $\approx 0.17$  eV) is used. It is clear, from Fig. 4(c), that the data at a temperature as low as 25 K can be fit very well with the ECFL line shape. In addition, in working with LSCO line shapes, we noticed that the data are characterized by a steady and rapid rise in intensity beyond  $-\omega = 0.25$  eV, a behavior different from that of Bi2212. We leave the full discussion of this non-universal behavior for future work. However, we find it exceptional that the current theory is able to describe the line shape of LSCO up to very high energy, as shown in Fig. 4(d).

**Kinks in the spectra:** The two independent energy scales  $\omega_0$  and  $\Delta_0$  are determined from our fit as  $\sim 0.5$  eV and  $\sim 0.1$  eV. These are natural candidates for the two main dispersion anomalies in the cuprates [12, 27] as in Fig. 5. Well-defined energy distribution curve (EDC: intensity curve at a fixed  $\vec{k}$  value) peaks disappear in a wide energy from  $\sim 0.3$  eV to  $\sim 1$  eV, as observed experimentally for the high energy kink [10, 12]. As this feature already exists in aux-FL, it cannot be associated with  $\Delta_0$  but rather with a higher energy scale  $\omega_0$ . The (numerical) dynamical mean field theory [28] can already account for this feature as can the present ECFL (analytical) theory.

Turning to the low energy ARPES kink at  $\sim 70$  meV, Figs. 5(c,d,e) illustrate the observed weak dispersion anomaly in the normal state data (c), reproduced in the ECFL theory (d) but not in the aux-FL theory (e). Here we use a visualization method for momentum distribution curve (MDC: intensity curve at a fixed  $\omega$  value), an object discussed primarily for low energy kinks. Thus this feature originates from the scale  $\Delta_0$ , it causes an increased asymmetry and the (blue) shift of the peak to high hole energy, when the third term in the caparison factor ( $\frac{n^2}{4} \frac{\xi_k - \omega}{\Delta_0}$ ) of Eq. 1 becomes important. To our knowledge, the ECFL theory is a unique analytical theory that has both these kink features arising from purely electronic (extreme) correlations.

In Fig. 5(f), we show the temperature dependence of the dimensionless peak skew or asymmetry, defined as  $(HL - HR) / (HL + HR)$ , where HR (HL) is the half-width at half maximum on the right (left) side of the peak. For this plot,  $\eta = 0.032$  eV is used [29]. Note that the skew of ECFL increases steeply with temperature as  $T^2$ , a prediction that would be worth exploring in the future, especially for  $T > 200$  K.

Further work is necessary to refine the picture suggested in this Letter. For example, as  $-\xi_k$  increases, the line shape becomes somewhat too asymmetric. Work is also in progress to apply the theory to two particle response as seen, e.g., in optical conductivity. We have checked that the bubble approximation (conductivity as a product of two  $G$ 's) shows an agreement in the order of magnitude of the frequency scale and the conductivity.

**Conclusions:** We have shown that it is possible to

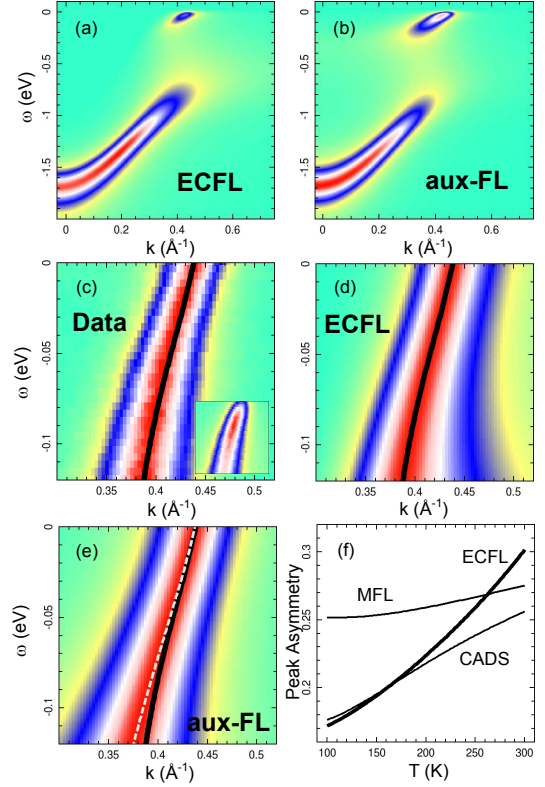


FIG. 5. Image plots of the spectral function for (a) the ECFL theory ( $\eta = 0.17$  eV), and (b) that of the auxiliary FL. (c) The data of Fig. 4(a) before (inset) and after (main) MDC normalization, by which each MDC is scaled and shifted to have minimum 0 (green) and maximum 1 (red). Blue corresponds to  $1/2$ . (d) The ECFL spectral function of (a), after MDC-normalization with MDC peak positions traced by black line. The black line in (c) is from (d). (e) The aux-FL spectral function of (b) after MDC-normalization. The MDC peak positions are traced by gray dashed line, while the black line is from (d). The bending such as shown by the black line here is commonly referred to as the kink. (f) The temperature dependence of the peak asymmetry compared for three different theories, rising as  $T^2$  for ECFL. Theory parameters for the calculation, apart from  $T$ , are taken from the fit of Fig. 2(a) for the ECFL, from the equivalent fit of Ref. 14 for the CADS, and from Ref. 23 for the MFL.

understand both ARPES data sets (laser or conventional) comprehensively, with identical physical parameters. The theory is very tolerant of the uncertainty in the background subtraction for the conventional ARPES data. Additionally, the theory satisfies the global particle sum rule, and contains two inter-dependent energy scales ( $\omega_0$  and  $\Delta_0$ ) that correspond well to the energy scales of the two kinks. Thus the simplest version of the ECFL theory using a small number of parameters, provides a framework to understand the ARPES line shape data for the normal state of the cuprates: *it works extremely well across techniques, samples and temperatures.*

SSRL and BNL are supported by the US DOE. The

work by GHG was supported partially by COR-FRG at UC Santa Cruz. BSS was supported by DOE under Grant No. FG02-06ER46319.

\* gweon@ucsc.edu

† sriram@physics.ucsc.edu

- 
- [1] J. D. Koralek, et al., Phys. Rev. Lett. **96**, 017005 (2006).  
 [2] W. Zhang, et al., Phys. Rev. Lett. **100**, 107002 (2008).  
 [3] In the sudden approximation, the ARPES intensity  $I(\vec{k}, \omega)$  is given by  $I(\vec{k}, \omega) = M(\vec{k})A(\vec{k}, \omega)f(\omega)$ . Here,  $\vec{k}$  is the momentum and  $-\omega$  is the energy of the final  $N - 1$  state, where  $N$  is the number of electrons in the initial state.  $A(\vec{k}, \omega) = \Im m G(\vec{k}, \omega - i0^+)/\pi$  is the single particle spectral function,  $M(\vec{k})$  is the dipole transition matrix element and  $f(\omega)$  is the Fermi-Dirac function. In this Letter, we set  $\hbar = 1$ , so that the wave vector and the (crystal) momentum are used interchangeably, as are the frequency  $\omega$  and the energy. We set  $\omega = 0$  at the chemical potential.  
 [4] B. S. Shastry, arxiv:1102.2858 (2011).  
 [5] B. S. Shastry, *Anatomy of the self energy* (preprint) (2011).  
 [6] It is easy to calculate the real part  $\Re \Phi(\omega) = -\frac{2}{\sqrt{\pi}\Omega_0} \exp\left(-\frac{\tau^2}{\omega_c^2}\right) \times \left[\omega_0\omega - 2(\omega^2 + \tau^2)D\left(\frac{\omega}{\omega_0}\right)\right]$  where  $D(x) = \frac{\sqrt{\pi}}{2}e^{-x^2}\text{erfi}(x)$  is the Dawson function.  
 [7] By secondary, we mean “intrinsic (i.e. part of  $A(\vec{k}, \omega)$ ) but dependent on the effective sample quality.”  
 [8] E. Abrahams and C. M. Varma, Proceedings of the National Academy of Sciences **97**, 5714 (2000).  
 [9] R. S. Markiewicz, et al., Phys. Rev. B **72**, 054519 (2005).  
 [10] W. Meevasana, et al., Phys. Rev. B **75**, 174506 (2007).  
 [11] Also, a minor  $k$ -shift of the theory was necessary ( $\sim 0.02$  Å) to match the slightly different  $k_F$  values reported in different experiments.  
 [12] J. Graf, et al., Phys. Rev. Lett. **98**, 067004 (2007).  
 [13] The effect of the finite angular resolution is significant only for the conventional ARPES data. However, the effect is minor and can be modeled well by an energy broadening.  
 [14] P. A. Casey, et al., Nat Phys **4**, 210 (2008).  
 [15] J. Koralek, Ph.D. thesis, University of Colorado (2006).  
 [16] A. Kaminski, et al., Phys. Rev. Lett. **86**, 1070 (2001).  
 [17] When it is allowed to vary but  $k$ -independent, it is 0.5 eV within  $\pm \sim 10$  %.  
 [18] C. G. Olson, et al., Phys. Rev. B **42**, 381 (1990).  
 [19] G. Gweon, J. W. Allen, and J. D. Denlinger, Phys. Rev. B **68**, 195117 (2003).  
 [20] A. Kaminski, et al., Phys. Rev. B **69**, 212509 (2004).  
 [21] T. Valla, et al., Science **285**, 2110 (1999).  
 [22] C. M. Varma, et al., Phys. Rev. Lett. **63**, 1996 (1989).  
 [23] A. Kaminski, et al., Phys. Rev. B **71**, 014517 (2005).  
 [24] T. Yoshida, et al., Journal of Physics: Condensed Matter **19**, 125209 (2007).  
 [25] T. Yoshida, Ph.D. thesis, University of Tokyo (2001).  
 [26] This means we attribute high  $k \gg k_F$  spectra to be purely background. One of the sources for the difference of this factor for different data sets examined here may be the presence of “superstructure replicas” in Bi2212 samples.  
 [27] A. Lanzara, et al., Nature **412**, 510 (2001).  
 [28] K. Byczuk, et al., Nat Phys **3**, 168 (2007).  
 [29] The asymmetry becomes stronger by more than a factor of 2, if  $\eta = 0.15$  eV is used, making the synchrotron data attractive for future investigation on this topic.